Supporting Information

Enhancement of Low Energy Sunlight Harvesting in Dye-Sensitized Solar Cells Using Plasmonic Gold Nanorod

Shuai Chang, *Quan Li*, *Xudong Xiao*, *King Young Wong* and *Tao Chen**

Supporting Text

Experimental

Materials: All chemical reagents were used without further purification. Hexadecyltrimethylammonium bromide (CTAB), silver nitrate, ascorbic acid and hydrogen tetrachloroaurate (III) hydrate 99.9% (metal basis) were purchased from Sigma Aldrich. Dye sensitizer cis-bis(isothicyanato)bis(2, 2'-bipyridyl-4, 4'-discarboxylato)-ruthenium (II)-bis-tetrabutylammonium, (coded as **N719**), TiO_2 paste (DSL 18NR-T) and iodide-based liquid electrolyte (HL-HPE) were purchased from Dyesol company. SiO_2 nanoparticles with 50 nm in diameter was purchased from Sigma-aldrich.

Synthesis of $AuNR@Ag_2S$: AuNRs (aspect ratio of 2.2, diameter and length at about 21 and 48 nm) were synthesized using a seed mediated method.[1] For the formation of Ag_2S shell on AuNR surface,[2] AuNR was firstly coated with a layer of Ag. Briefly, 10 mL of AuNRs was centrifuged at speed of 10k rpm for 10 min to remove the large excess CTAB, it was then diluted to 10 mL by DI water for the following reactions. For coating Au layer with different thicknesses of Ag and thus Ag_2S (2 nm, 3.7 nm and 6 nm), 0.5 mL, 1mL and 2 mL $AgNO_3$ (1mM in DI H_2O) were added to the 10 mL AuNRs solution, respectively. Thereafter, 0.1 mL, 0.4 mL and 0.8 mL ascorbic acid (0.1 M in H_2O) were added to each of the solution. The pH of the solution was adjusted to 8 by NaOH (0.1 M in H_2O) to start the reaction and ensure a slow reaction rate. After a few miniatures, Na_2S (10 mM) was added (20 μL, 30 μL, 50 μL) to the solution to transform Ag to Ag_2S. It is noted that dielectric constant of Ag_2S is 6, much larger than that of water, 1.33, though the aspect ratio remain nearly unchanged, Ag_2S encapsulating on the *entire* surface of AuNR would cause redshift of both the transverse and longitudinal peaks (Fig. 1d and Fig. S5).

Different amount of AuNR@Ag$_2$S were added to TiO$_2$ paste to achieve final concentrations of AuNR@Ag$_2$S of 0.88%wt, 1.66%wt, 2.05%wt. The mixed pastes were sonicated at 60 $^\circ$C for 4 hrs before use.

Ag nanoparticles with diameter of about 60 nm was synthesized through a citrate reduction method.[3] Briefly, 36 mg of AgNO$_3$ was dissolved in 200 mL H$_2$O and heated at 120 $^\circ$C for 10 min under vigorous stirring. 4 mL of sodium citrate (1% wt) was then added and heating was extended to another 30 min, followed by cooling down to room temperature naturally. After that, Ag@Ag$_2$S was synthesized through adding 100 μL of Na$_2$S (2 mM) into 10 mL of as-synthesized Ag nanoparticles under vigorous stirring (Fig. S8). To prepare Ag@Ag$_2$S/TiO$_2$ paste, 1 mL of Ag@Ag$_2$S nanoparticles was concentrated to 400 μL by centrifugation. A portion of 100 μL was added 500 mg TiO$_2$ paste for the plasmonic paste.

Device fabrication: A doctor-blade technique was utilized to produce photoanodes films. Briefly, transparent conducting glass (SnO$_2$:F, FTO glass, 15 Ω^{-1}) was cleaned by sonication in ethanol, acetone and DI water for 20 min during each washing step. Then 6 μm or 11μm thick TiO$_2$, AuNR@Ag$_2$S/TiO$_2$ or Ag@Ag$_2$S/TiO$_2$ electrodes were doctor-bladed onto FTO surfaces for different devices. The pastes were then relaxed at room temperature for 3 min before heating at 450 $^\circ$C for 60 min to remove polymers. After cooling down to room temperature, the electrodes were immersed in 0.3 mM N719 dye in acetonitrile/tert-butyl alcohol (1:1, v/v) at room temperature for 16 hrs, followed by briefly rinsing with ethanol and drying in air to remove the non-adsorbed dyes. It should be noted that for the 11μm plasmon paste, it is composed of 3 μm bottom layer with pure TiO$_2$ nanoparticles, and 8 μm of top layer with AuNR@Ag$_2$S (0.88%wt) in TiO$_2$.

Platinum counter electrodes were prepared by sputtering method at 20 mA for 60 s at a power 150 W. Two holes (0.75 mm in diameters) were pre-drilled in the FTO glass for introducing electrolyte. After that, dye-adsorbed TiO$_2$ electrode and counter electrode were stacked and sealed with 60 μm thermal-plastic parafilm spacers at about 120 $^\circ$C. Iodide-based liquid electrolyte (HL-HPE, 0.1 M LiI, 50 mM I$_2$ and 0.6 M DMPII) was introduced into the sandwich cells through the drilled holes in the Pt electrode. After that, it was sealed by parafilm and covering glass at elevated temperature. The effective areas of all the photoanodes are 0.24 cm^2.

Characterizations: The cross-section of anode film was characterized on a scanning electron microscopy (FEI Quanta 400 FEG microscope). TEM images of the as-synthesized

nanoparticles were collected from Philips CM120 microscope operating at 120 kV. UV-Vis absorption and reflection of the colloidal solutions and anode films with and without dye adsorption were carried out using Hitachi U-3501 UV–visible/NIR spectrophotometer. The current-voltage (*J-V*) characteristics of the assembled cells were measured by a semiconductor characterization system (Keithley 236) at room temperature in air under the spectral output from solar simulator (Newport) using an AM 1.5G filter with a light power of 100 mW/cm^2. Electrochemical impedance spectroscopy (EIS) was recorded under one sun illumination over a frequency range of 0.1-105 Hz with an AC amplitude of 10 mV by using electrochemical workstation (CHI 660D). The parameters were calculated from Z-View software (v2.1b, Scribner AssociatNe, Inc.). IPCEs of DSSCs were recorded in Solar Cell QE/IPCE Measurement System (Zolix Solar Cell Scan 100) using DC mode.

Supporting discussions

1. To further investigate the scattering effect, we used SiO$_2$ (50 nm in diameters) to replace AuNR@Ag$_2$S with the same concentration for investigation   (denoted as Device *TiO$_2$/SiO$_2$-1*). The PCE is 4.4%. Since of some TiO$_2$ nanoparticle are replaced by SiO$_2$ nanoparticles, the ICPE at around 370 nm is decreased when compared with device **1**. Further increasing the concentration of SiO$_2$ nanoparticles (Device *TiO$_2$/SiO$_2$-2*, increased by four times), the IPCE at blue region (around 370 nm) shows considerable improvement, indicating the scattering effect of SiO$_2$ nanoparticles (Fig. S9). Clearly, AuNR@Ag$_2$S is more efficient than SiO$_2$ due to the large scattering cross section. However, the IPCE at 600-720 nm remain nearly unchanged in both concentrations, which is different from AuNR@Ag$_2$S nanoparticles in the TiO$_2$ network (device **1** *vs*. device **3**). There are three possible mechanisms for the V_{oc} increase in SiO$_2$ incorporated DSSCs. 1) It has been found that SiO$_2$ nanoparticles can facilitate ion transport of electrolyte in DSSCs.[4] In the current case, SiO$_2$ nanoparticles are distributed in TiO$_2$ nanoparticle network in DSSCs. Therefore, SiO$_2$ nanoparticle can speed up the diffusion of electrolyte, thus facilitating electron exchange reaction and increasing V_{oc}. 2) SiO$_2$ contacted with TiO$_2$ nanoparticles would retard the recombination at the interface of TiO$_2$/electrolyte, i. e. suppress the back electron transfer from TiO$_2$ to electrolyte, this can also increase V_{oc}.[5] 3) SiO$_2$ scattering improved bandgap transition can also lead to a lift up of quasi-Fermi level of electrons in TiO$_2$ which thus increase the V_{oc} since it is defined as the difference between the potential of redox electrolytes and the quasi-Fermi level of electrons in TiO$_2$. In addition, the reduced dark current would contribute to the increased V_{oc} (Fig. S16). However, too much SiO$_2$ nanoparticles in the DSSCs lead to both TiO$_2$ nanoparticles and

loaded dye molecules becoming less, thus giving birth to degraded V_{oc} (device 9).

2. The anode films were studied by SEM with Energy-dispersive X-ray spectroscopy (EDX). Fig. S11 shows the SEM images of anode film of device 3. Since the size of TiO_2 in our experiment is 20 nm, while the AuNR@Ag$_2$S is about 23 nm and 50 nm in diameter and length, the two types of nanoparticles can be easily differentiated. It can be seen that the morphology of AuNR@Ag$_2$S remain nearly unchanged and there are no aggregation of AuNR@Ag$_2$S nanoparticles . Since TiO_2 is stable upon annealing at 450 °C, here we only test the stability of AuNR@Ag$_2$S. This design is also under the consideration that the concentration of AuNR@Ag$_2$S in TiO_2 anode film is too low to be detected for a clear demonstration. For Energy-dispersive X-ray spectroscopy (EDX) characterization, a layer of AuNR@Ag$_2$S is deposited on FTO substrate and annealed the same as the preparation of anode films. The result shows that there are Au, Ag and S element, with some other elements coming from conducting glass (Fig. S12). This result, coupling with the above SEM images of the anode film, demonstrates the both the morphology and elements are remained in the devices.

3. Optical properties of AuNR@Ag$_2$S on glass. The optical absorption of AuNR@Ag$_2$S on a piece of glass was prepared drop casting. The spectrum (Fig. 13) is similar shape of AuNR@Ag$_2$S colloidal. The redshift of absorption result from aggregation during sample preparation.

4. Regarding the photon loss in AuNR@Ag$_2$S-incorporated devices. In DSSC, incident photon-to-electron conversion efficiency (IPCE) is a product of light harvesting efficiency (η_{lh}), electron injection efficiency (η_{inj}) and electron collection efficiency (η_{col}). In this work, addition of AuNR@Ag$_2$S increases η_{lh} as indicated in Fig. 4a and decreases η_{col} due to the increased series resistance, we assume that η_{inj} remains unchanged. From Fig. 4a, the light absorption of device **3** is increased by 32.0% when compared with that of device **1**. However, the J_{sc} improvement is only 26.28%. This difference in J_{sc} (IPCE) increase and light absorption increase can be considered as the maximum photon loss in form of "waste heat". Further, in device **4**, the absorption is increased by 38.4% while the J_{sc} improvement is only 12.6%. The less improved J_{sc} should be due to the decreased η_{col}. High concentration of AuNR@Ag$_2$S in TiO_2 nanoparticle network would lead to more pronounced series resistance for smaller η_{col}. Therefore, in the devices, the photon loss is dependent on the concentration of AuNR@Ag$_2$S in the anode films.

We also performed simulation to investigate the photon loss as a result of interband transition

using FDTD Solutions 7.5, developed by Lumerical Solutions, Inc. In the simulations, an electromagnetic pulse ranging from 400 to 1200 nm was launched into a box containing a target nanostructure. A mesh size of 0.5 nm was applied in the simulations. The morphological parameters of the nanostructures were set according to the average sizes measured from TEM images. Au nanorod was treated as a cylinder capped with a hemisphere at each end (right Figure). The diameter and total length of the core (AuNR) are 21.08 nm and 47.97 nm, respectively. The Ag_2S shell thickness is 2 nm. The dielectric functions of gold and silver sulfide were taken from previously measured values.[6][7] The calculation results show that ~98% of light absorption at interband converts to waste heat. However, solar thermal conversion at longer wavelengths become smaller; this reduced light-to-heat conversion efficiency could also contribute to the increase in η_{lh}.

5. To measure the dye loading capacities of device **1** to **4**, the dye adsorbed anode films were immersed in NaOH solution (0.1 M in H_2O) for 12 hrs. Results are shown in Fig. S6.
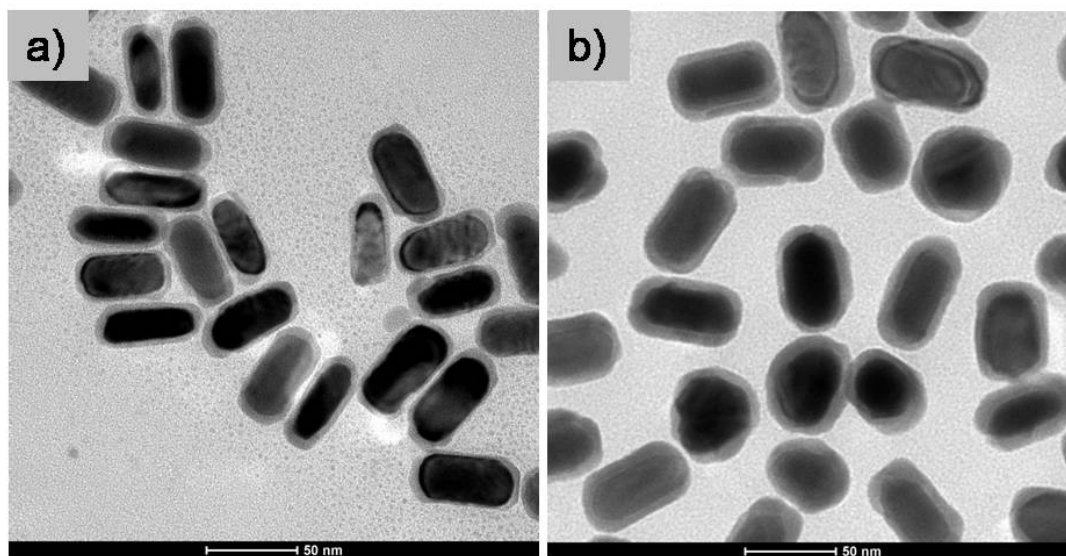
Fig. S1 TEM images of AuNR@Ag_2S with shell thickness of 3.7 nm (a) and 6 nm (b).
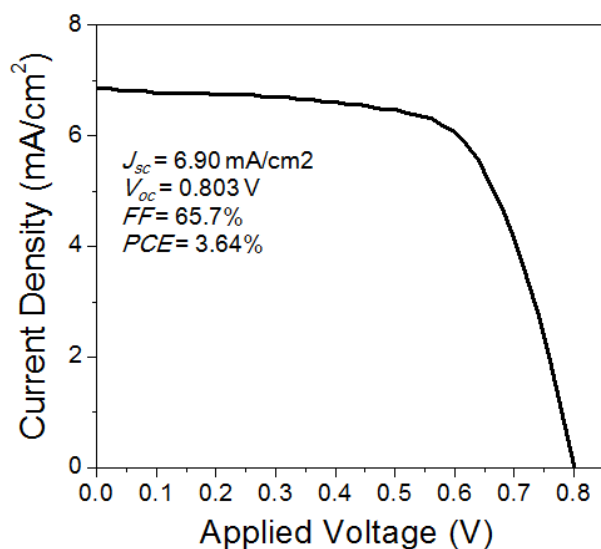
Fig. S2 *J-V* curve of DSSC with naked (without Ag$_2$S encapsulation) AuNR-incorporated TiO$_2$ nanoparticle anode.
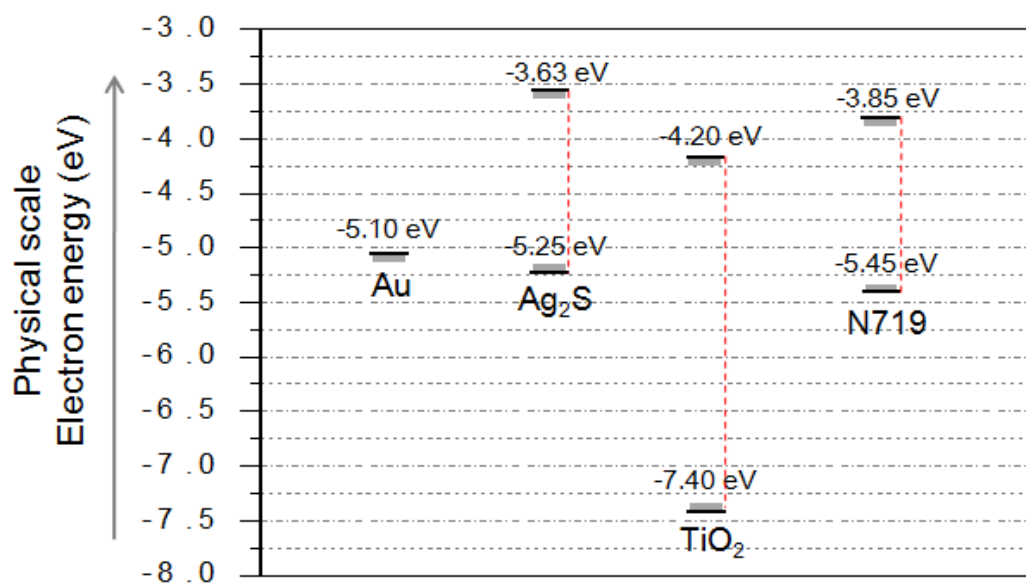
Fig. S3 Band alignment of Au, Ag$_2$S TiO$_2$ and N719.
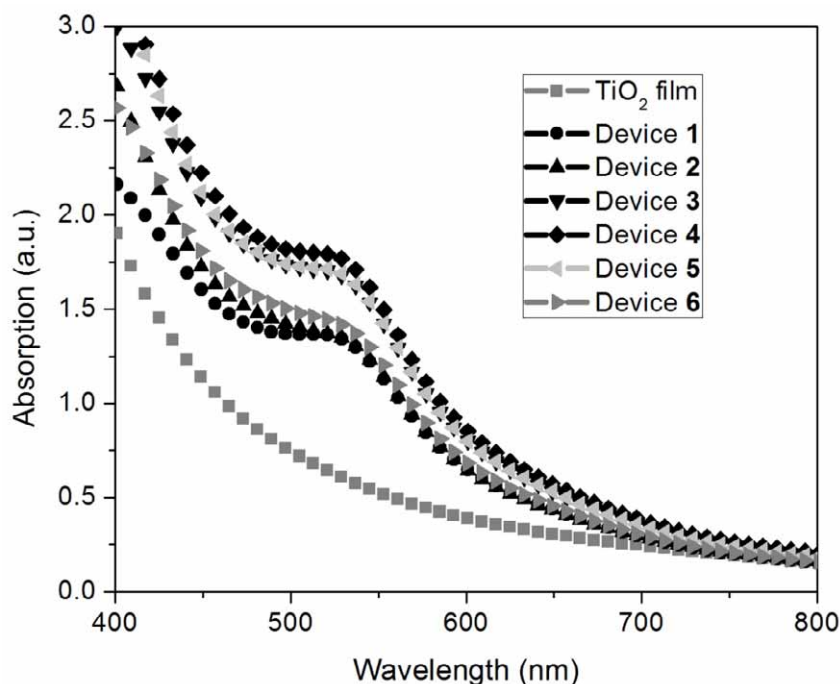
Fig. S4 UV-Vis absorption of the TiO$_2$ film and anode films of device **2**, **5** and **6**, those of device **1, 3** and **4** are also plotted for easy comparison.
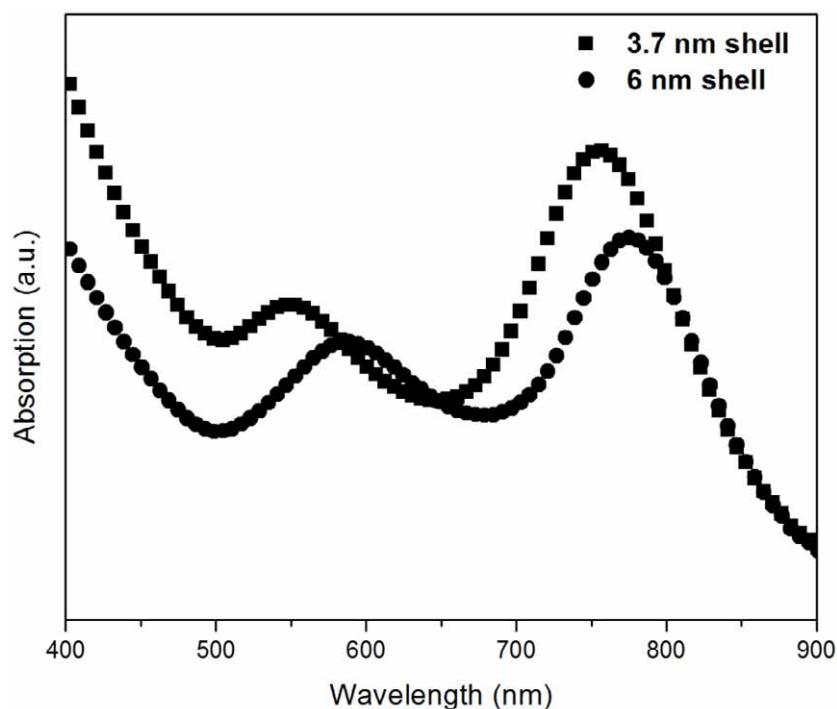
Fig. S5 UV-Vis-NIR spectra of AuNR@Ag$_2$S with shell thickness of 3.7 and 6 nm. The two peaks at shorter and longer wavelengths for each of the sample are transverse and longitudinal plasmon absorptions.
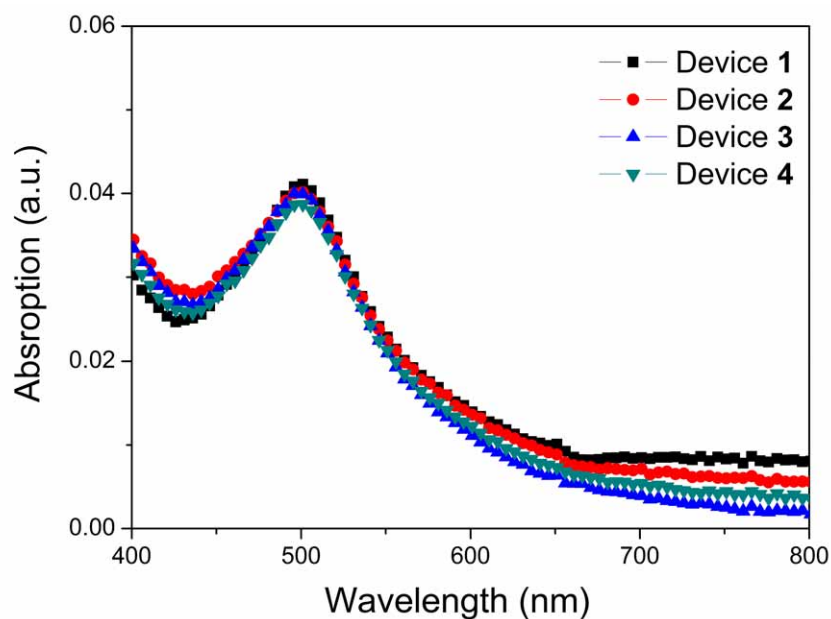
Fig. S6 relative dye loading capacities of device **1** to **4**.
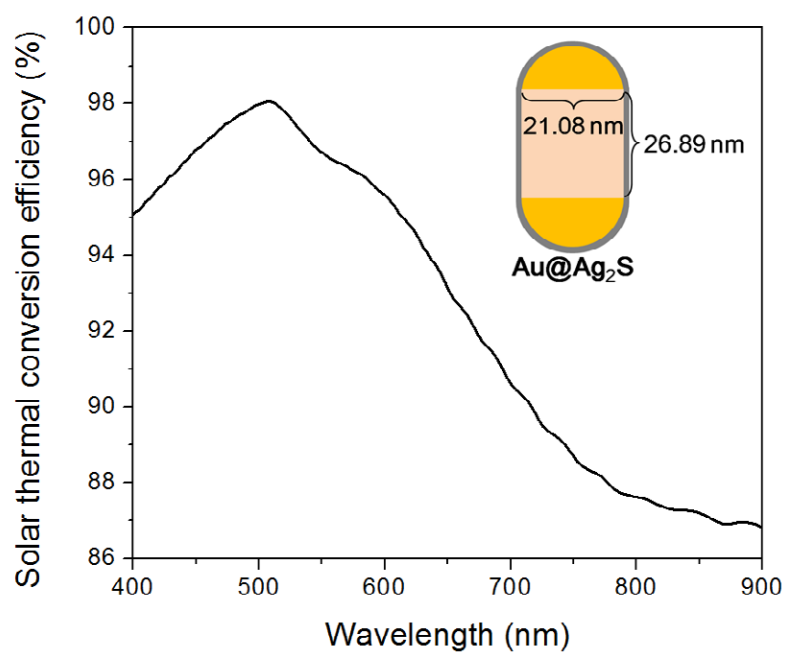
Fig. S7FDTD calculation of solar thermal energy conversion efficiency of AuNR@Ag$_2$S.
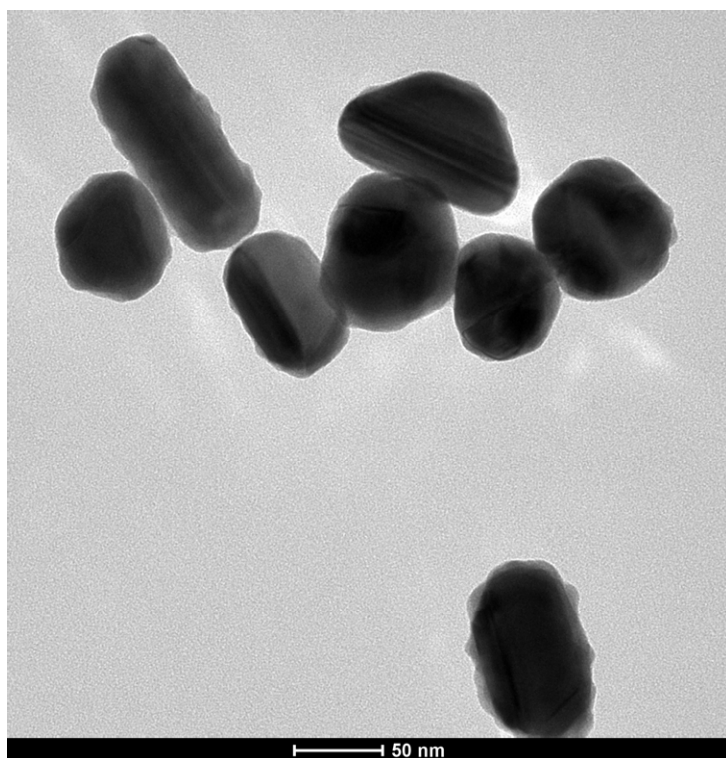
Fig. S8 TEM image of the as-synthesized Ag@Ag$_2$S nanoparticles.
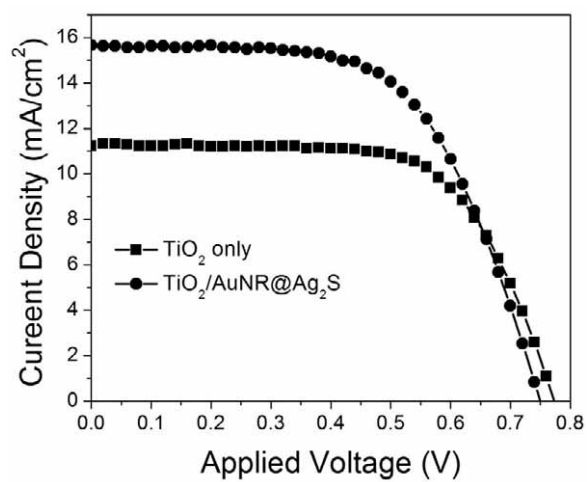
Fig. S9 *J-V* curves of devices with 11 μm of anode films.
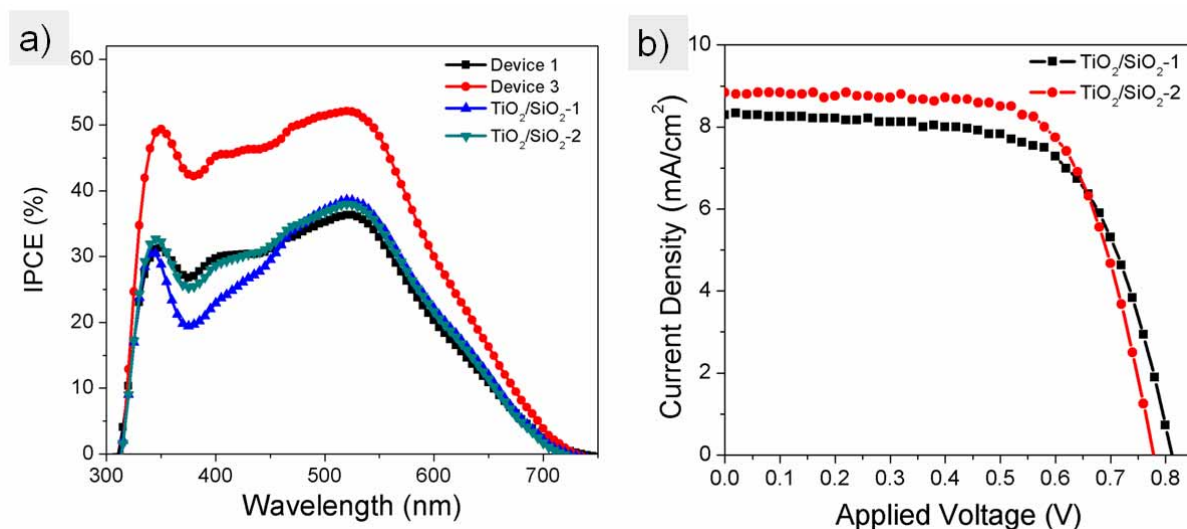
Fig. S10 IPCE of DSSCs with different concentration of SiO_2 in TiO_2 particles (a), those of device **1** and **3** are also plotted for easy comparison. *J-V* curve of devices with different concentration of SiO_2 (b).
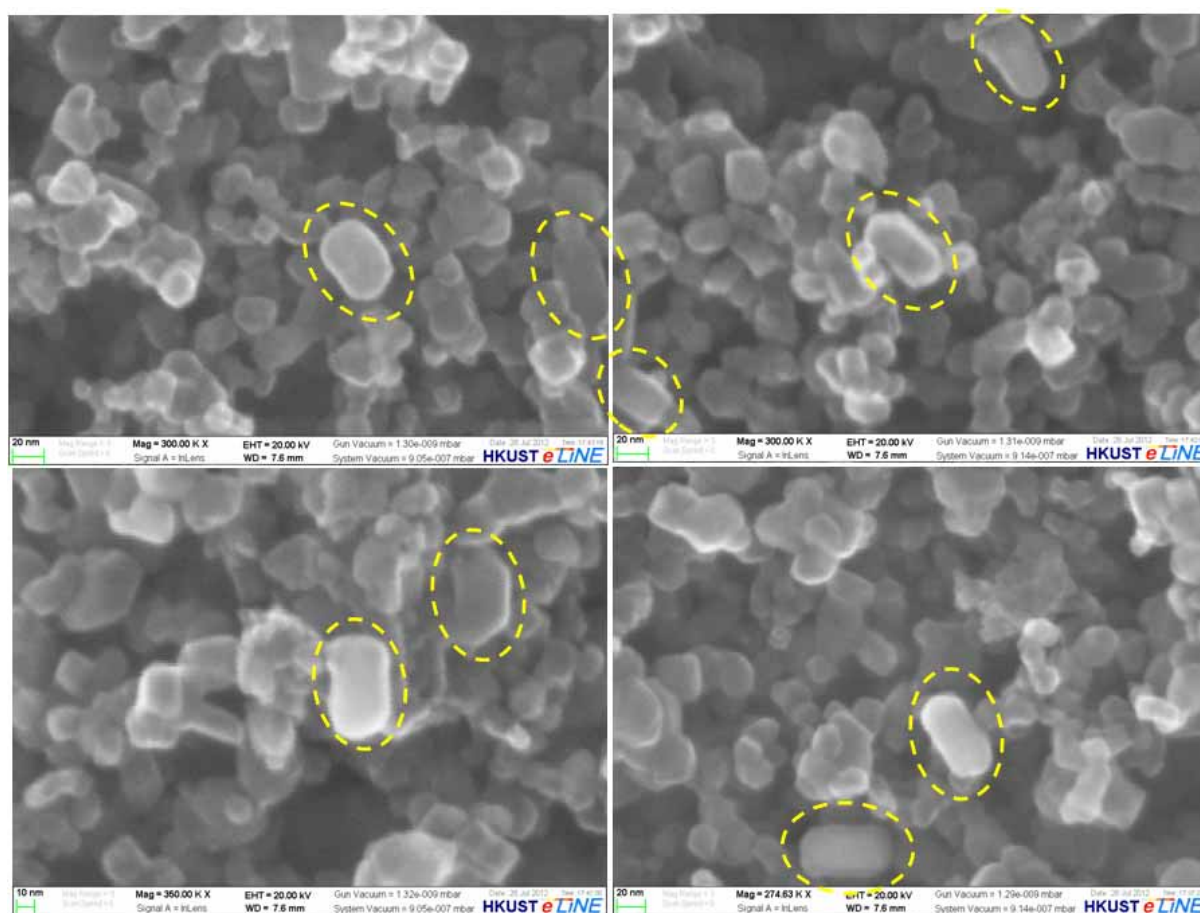
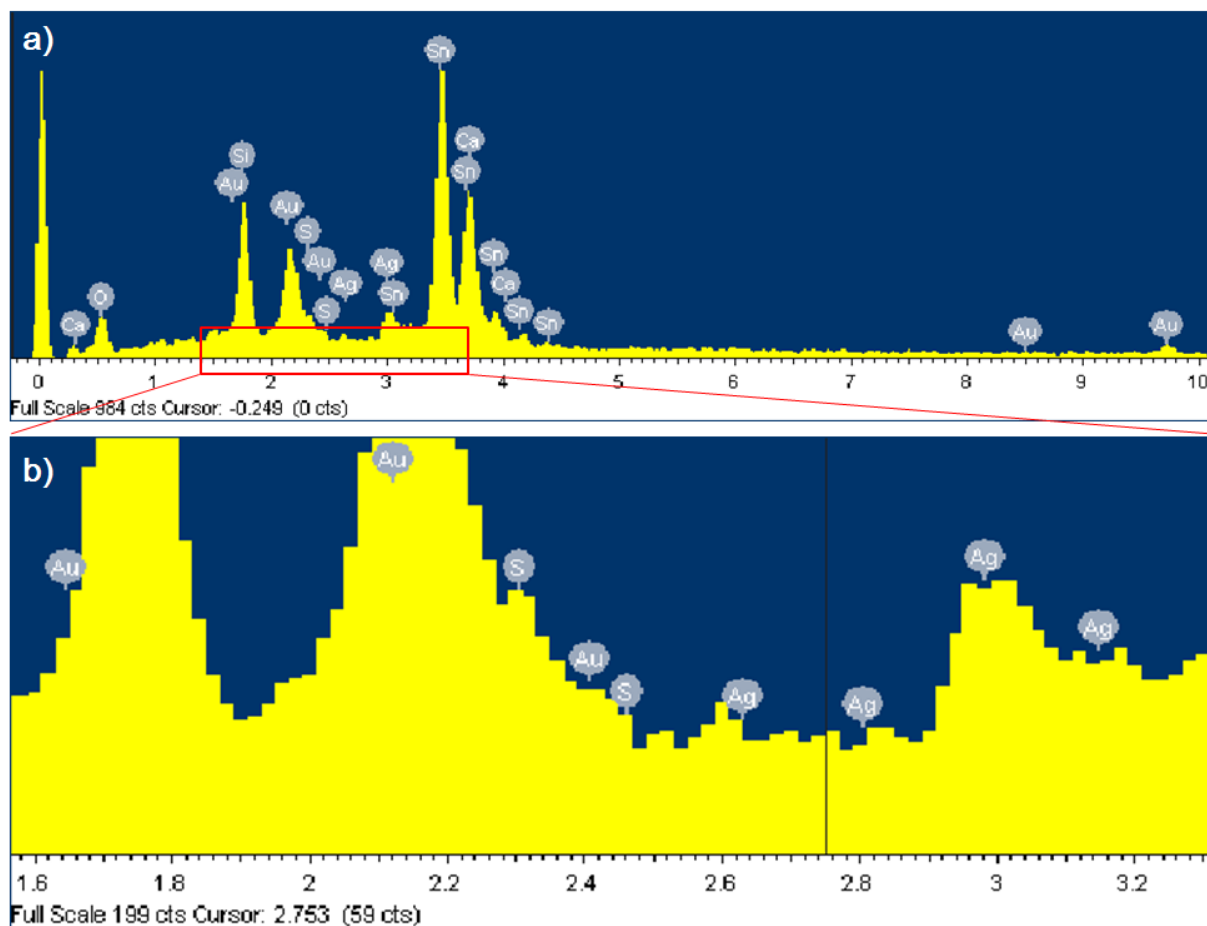**Fig. S11** SEM images of anode film of device **3**, $AuNR@Ag_2S$ nanoparticles are circled for easy observation.

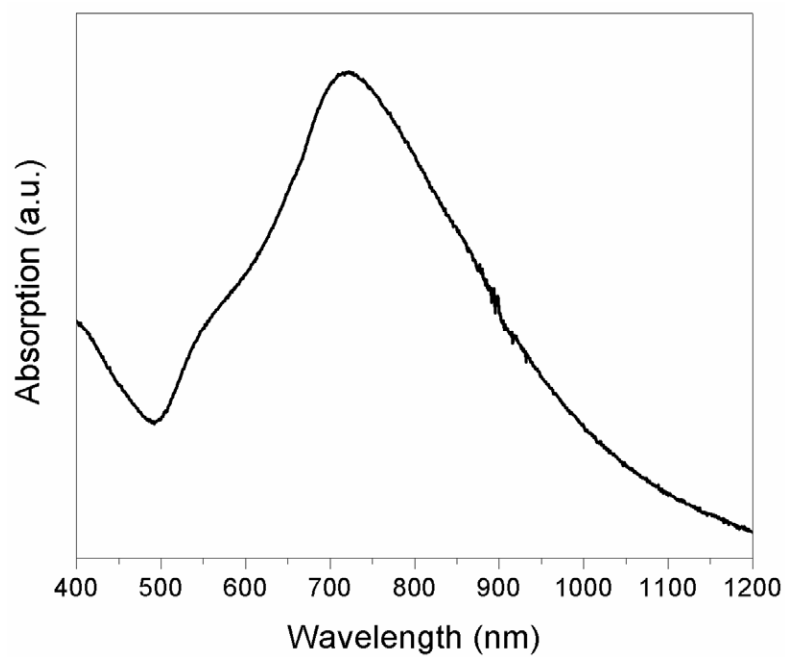**Fig. S12** EDX spectra of high temperature annealed AuNR@Ag$_2$S on glass/FTO surface.

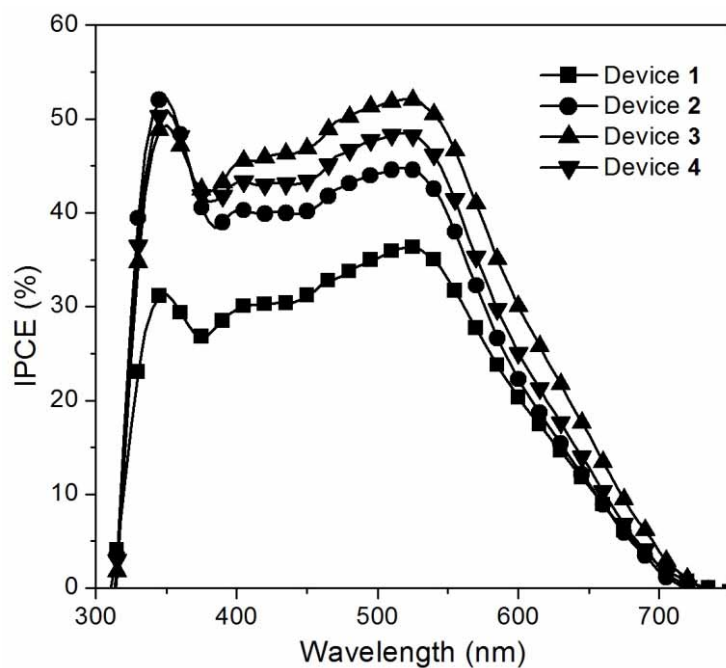**Fig. S13** UV-Vis-NIR absorption of the AuNR@Ag$_2$S on FTO surface.

Fig. S14 IPCE of device **1** and **3**, those of device **2** and **4** are also plotted for easy comparison.
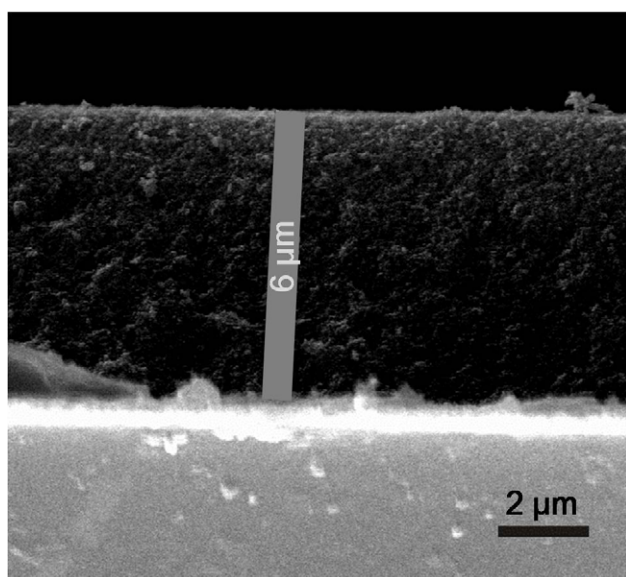

Fig. S15 SEM image of cross-section of TiO_2 anode film, the thickness is measured to be 6 μm.
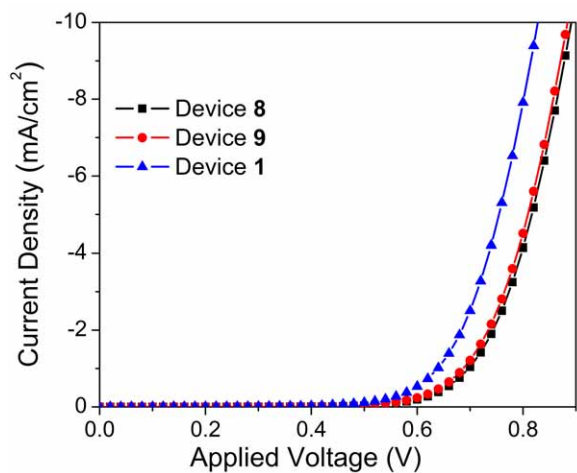
Fig. S16 *J-V* profiles of device **1**, **8** and **9** under darkness.

Supporting references:
[1] A. Gole, C. J. Murphy, *Langmuir* **2008**, 24, 266.
[2] M. Z. Liu, P. Guyot-Sionnest, *J. Mater. Chem.* **2006**, 16, 3942.
[3] P. C. Lee, D. Meisel, *J. Phys. Chem.* **1982**, 86, 3391.
[4] M. Berginca, M. Hočevar, U. Opara Krašove, A. Hinsch, R. Sastrawan, M. Topiča, *Thin Solid Films* **2008**, 516, 4645.
[5] H. J. Son, X. W, Wang, C. Praittichai, N. C. Jeong, T. Aaltonen, R. G. Gordon, J. T. Hupp, *J. Am. Chem. Soc.* **2012**, 134, 9537.
[6] P. B. Johnson, R. W. Christy, *Phys. Rev. B*, **1972**, 6, 4370;
[7] J. M. Bennett, J. L. Stanford, E. J. Ashley, *J. Opt. Soc. Am.*, **1970**, 60, 224.